*Peopling the Landscape of Çatalhöyük: Reports from the 2009–2017 Seasons*

Edited by

Ian Hodder

# Colour figures for Chapter 2. Disentangling the palaeoenvironmental reconstructions of Çatalhöyük

Gianna Ayala, John Wainwright, Jerry M. Lloyd, Joanna R. Walker,
Rachel Hodara Nelson, Melanie Leng, Chris Doherty and Michael Charles

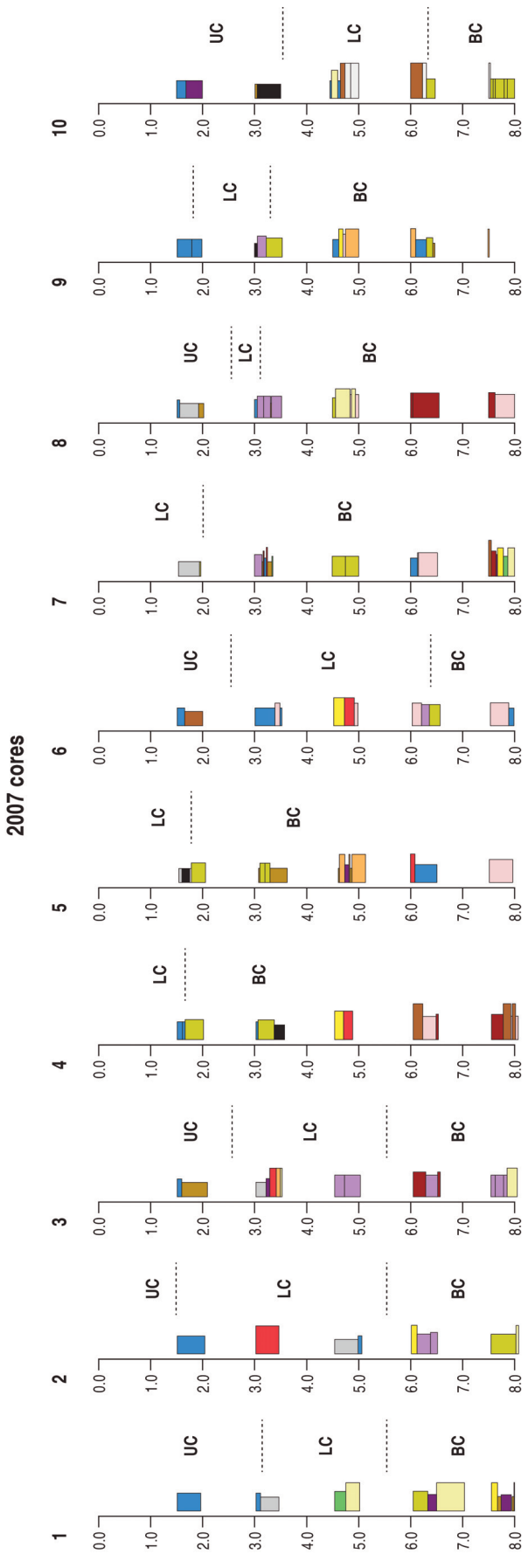


*Figure 2.2. a) Stratigraphic sequence 2007 (Ayala et al. 2017: fig. 2a).*

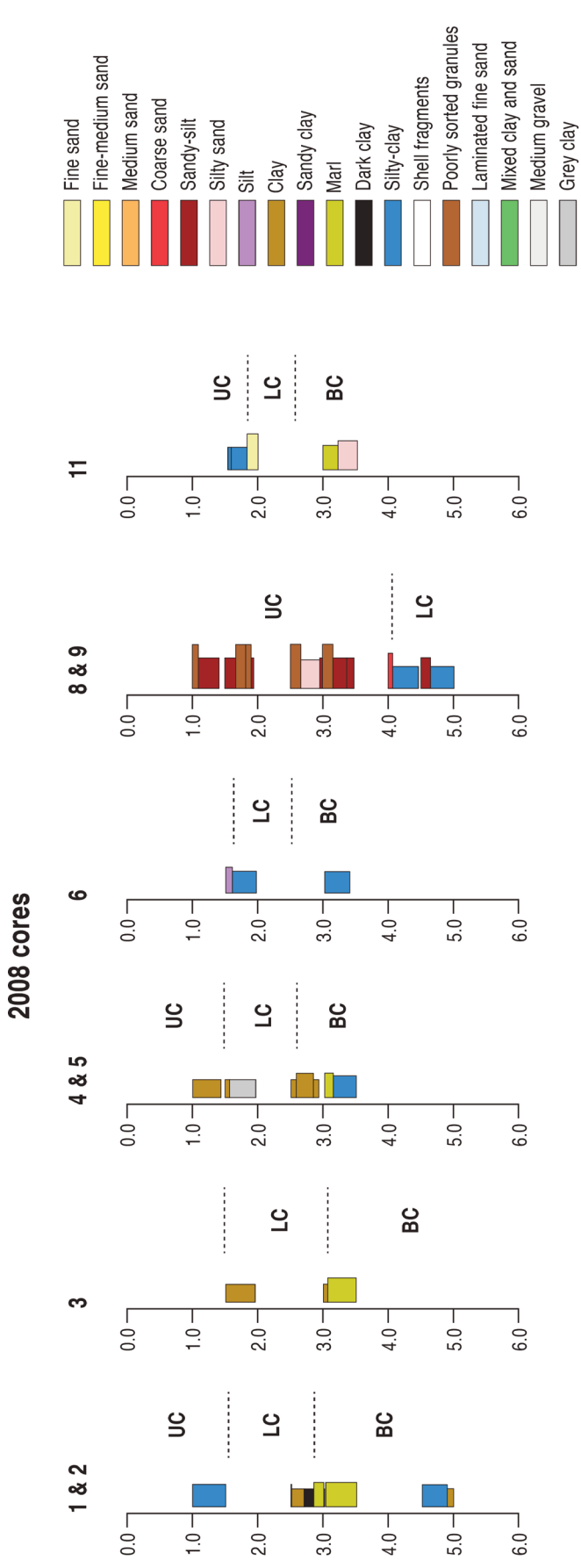


*Figure 2.2. b) Stratigraphic sequence 2008 (Ayala et al. 2017: fig. 2b).*

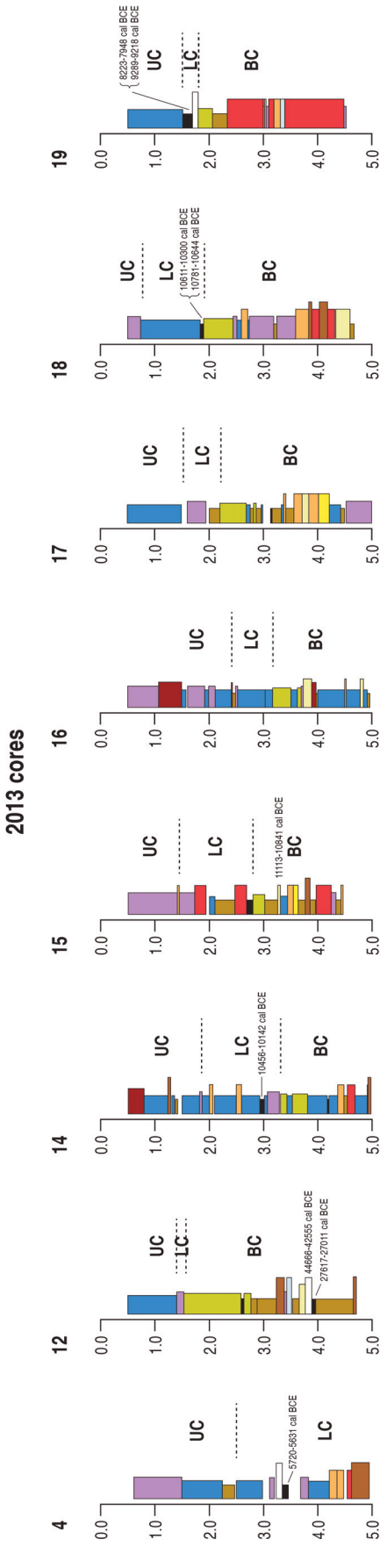


*Figure 2.2. c) Stratigraphic sequence 2013 (Ayala et al. 2017: fig. 2c).*

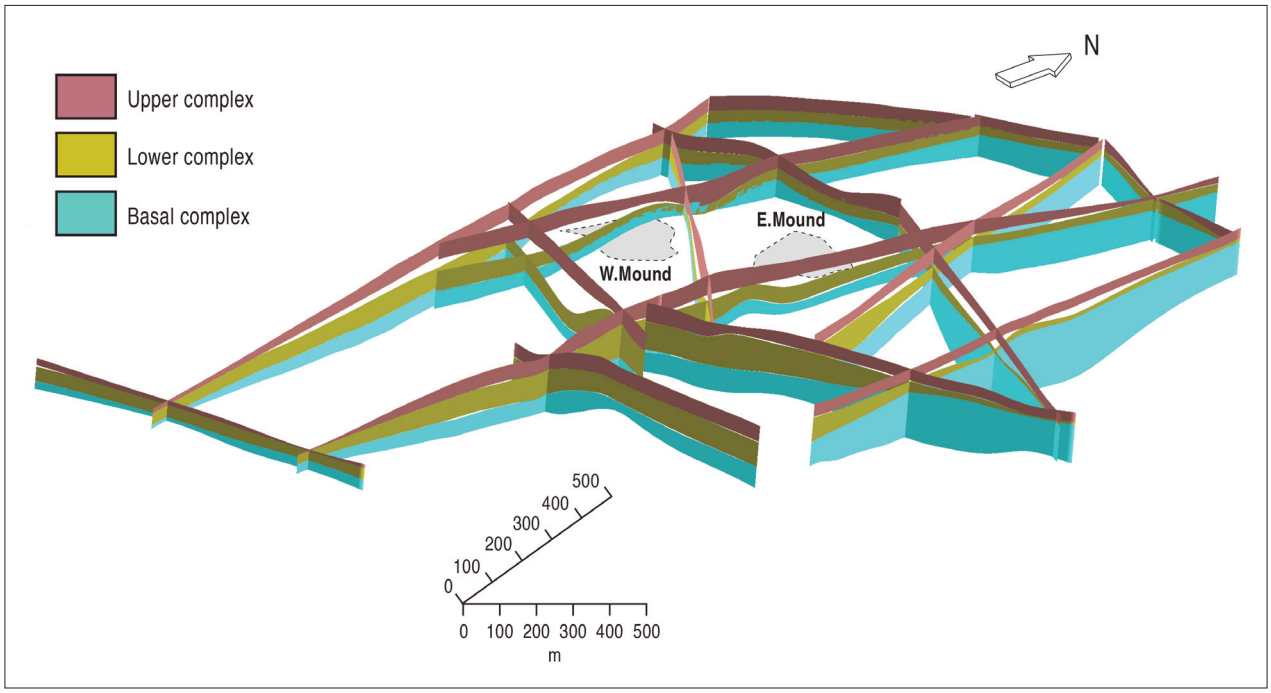


*Figure 2.3. Fence diagram of the 2007–2013 cores (Ayala et al. 2017: fig. 5). The sequence at Çatalhöyük is here summarised: full sedimentological description and supporting evidence is available in Ayala et al. 2017.*

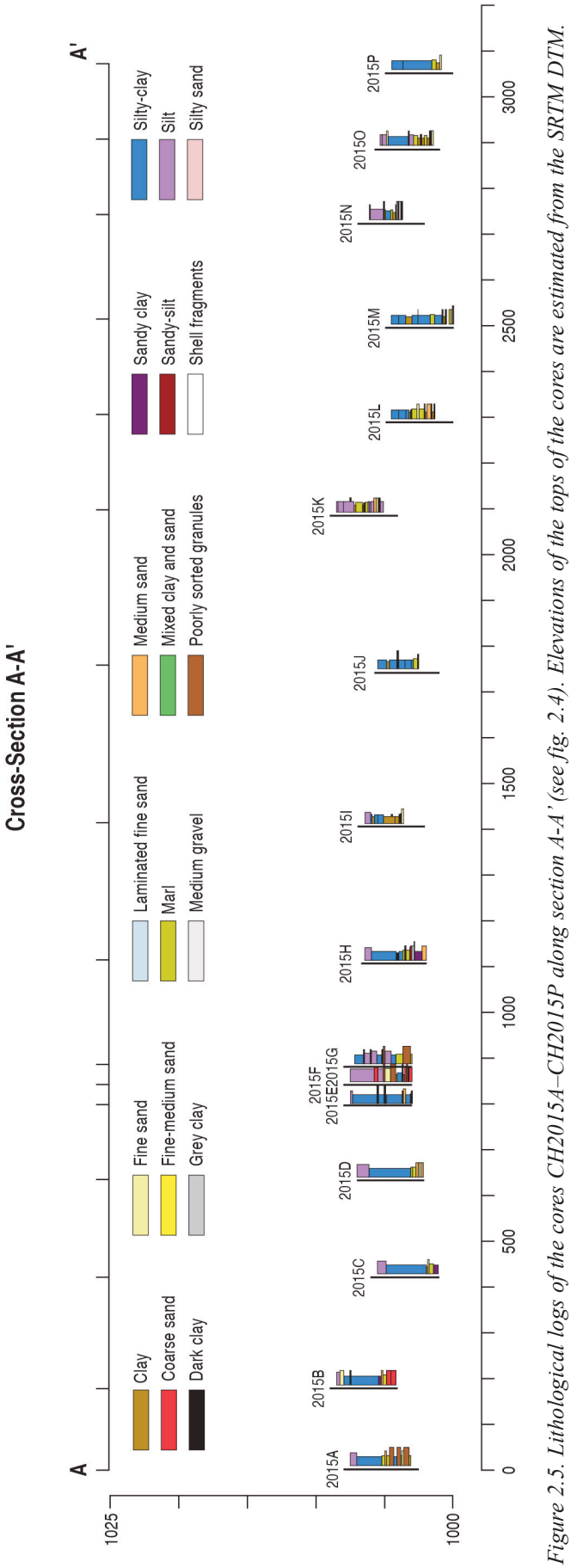


*Figure 2.5. Lithological logs of the cores CH2015A–CH2015P along section A-A' (see fig. 2.4). Elevations of the tops of the cores are estimated from the SRTM DTM.*

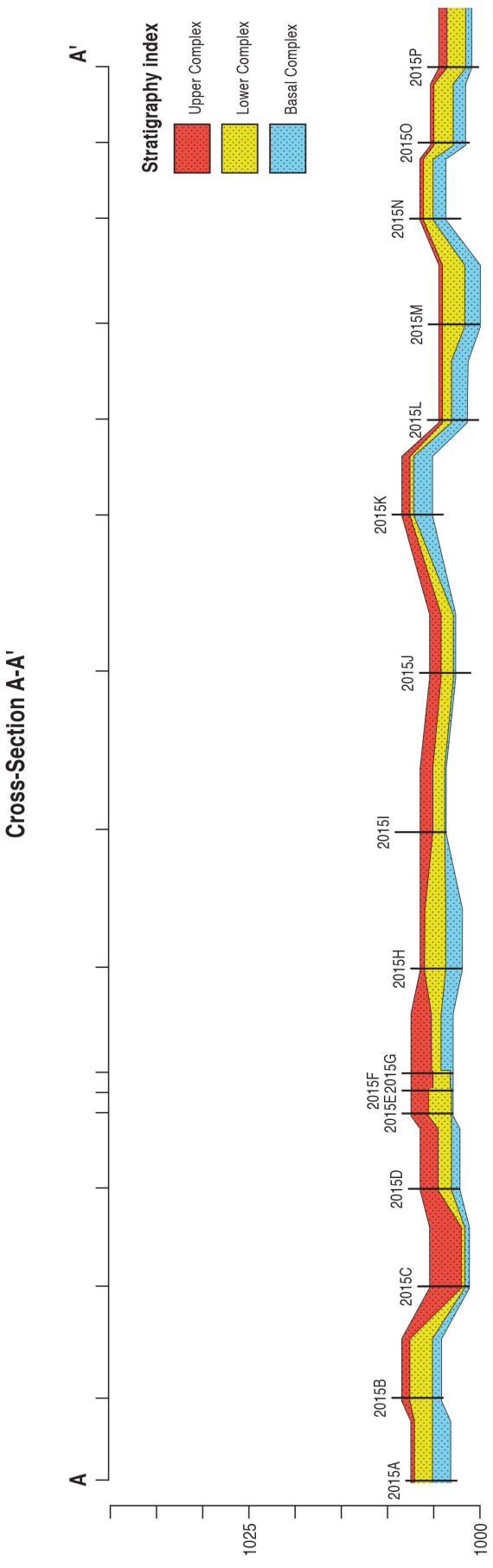


*Figure 2.6. Sedimentological correlation of the cores CH2015A–CH2015P along section A-A' (see fig. 2.4). Elevations of the tops of the cores are estimated from the SRTM DTM.*

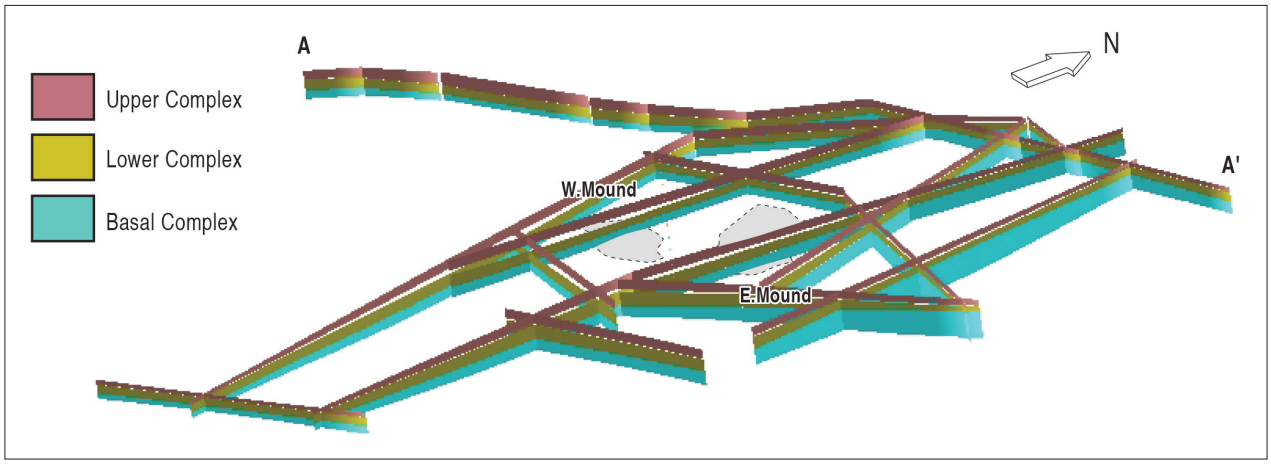


*Figure 2.7. New fence diagram showing the impact of the new cores CH2015A-A' (compare with fig. 2.3) in the landscape interpretation.*

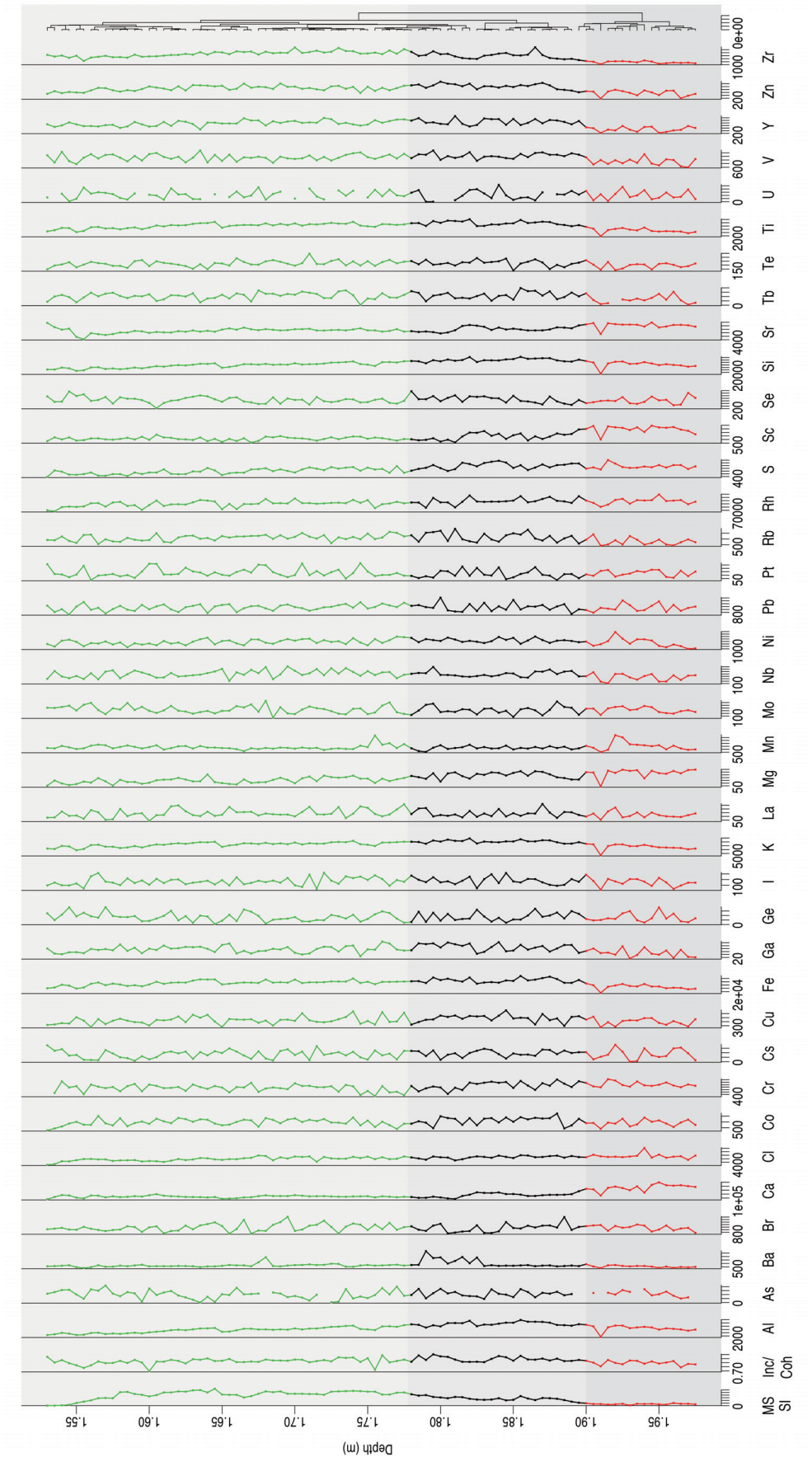


*Figure 2.8. Example of Micro-XRF analysis of core CH2015K. First column on the left, MS SI= magnetic susceptibility ($10^{-5}$ SI), while the second column, Inc/Coh ratio provides a proxy for organic matter content (Croudace, Rothwell 2015). Remaining panels are area estimates for the different elements analysed, showing the relative contents of each. The dendrogram on the right is based on hierarchical clustering (calculated using the rioja package in R: Juggins 2019) and shows that the marl is significantly different from either the Dark Clay or the Lower Complex silt. The two latter deposits are more closely related to each other. Lines are coloured according to lithology: red is the marl, black is the Dark Clay and green is the Lower Complex silt.*

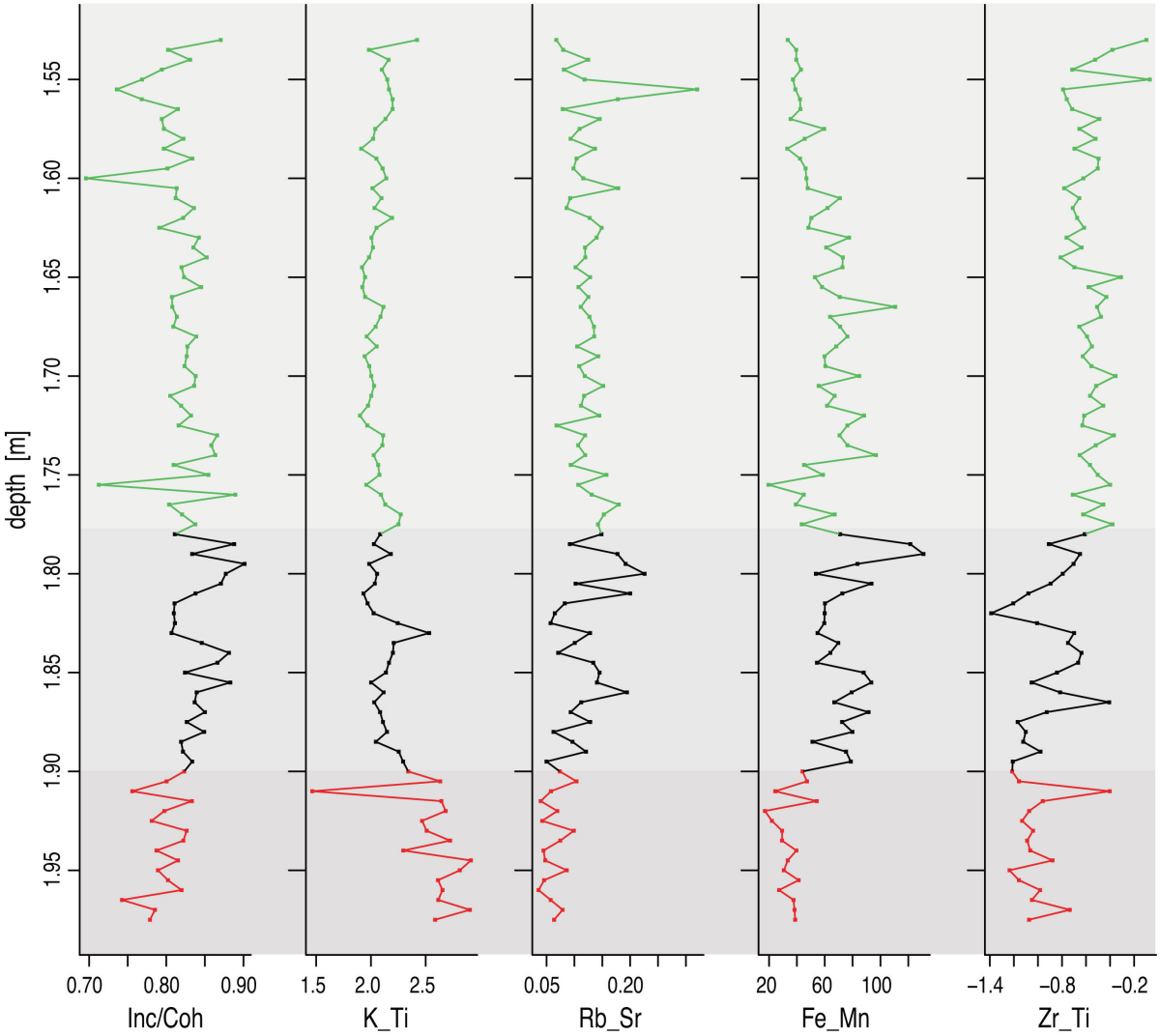


*Figure 2.9. Series of ratios of micro-XRF analyses used in previous studies for palaeoenvironmental interpretation. Lines are coloured according to lithology: red is the marl, black is the Dark Clay and green is the Lower Complex silt.*

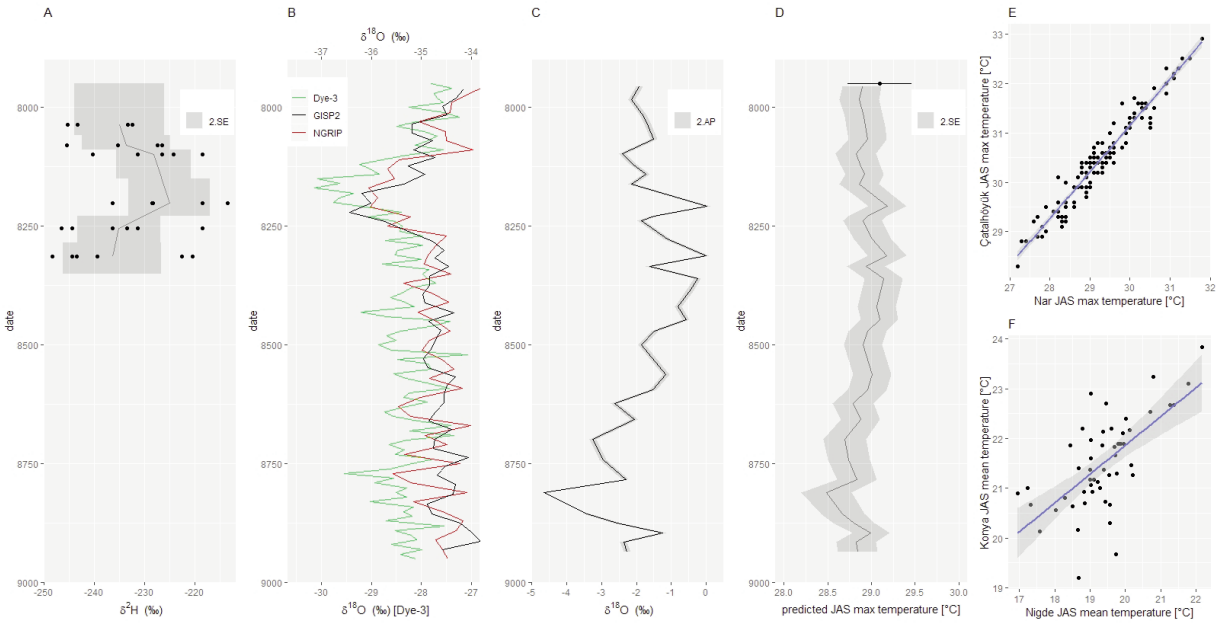


*Figure 2.11. Comparison of the $\delta^2H_{18:0}$ proxy of Roffet-Salque et al. (2018) with global and regional climate records. This plot uses a window from 9000 to 7800 calibrated B.P. to place the proxy data in a longer-term context consistent with the discussion in the text here: (a) replots the data of figure 1D in Roffet-Salque et al. (2018) using shading to show the 2-SE variation of data around the mean (solid line); original data points are plotted at the midpoint of the archaeological phase, but shading is shown vertically to demonstrate the full uncertainty of the Bayesian estimates of these phases. There is clear overlap between the phases, and variability is more important than mean values; (b) water $\delta^{18}O$ values of three Greenland ice cores (Stuiver et al. 1995; NGRIP Dating Group 2006; Vinther et al. 2006; Rasmussen et al. 2007) used to demonstrate the onset and duration of the 8.2kya event; (c) $\delta^{18}O$ record from the sediments in Nar Lake (Jones et al. 2005), ~150 km from Çatalhöyük, which provides the best available regional information for climate proxies. Shaded area shows 2× analytical precision (AP) of the measurements; (d) estimate of summer maximum temperature for Nar Lake, based on the proxy derived by Jones et al. (2005) from modern climate measurements. The shaded area is 2 SEs, using a RMS combination of the uncertainties from the measurement analytical precision and the SE from the proxy model. The point and error bar at the top of the plot show the mean and 2-SE range for the 1961–1990 climatic observations; (e): relation between CRU TS4.01 (Harris et al. 2014) reconstructed JAS maximum temperature 1901–2016, $r^2=0.943$, $p < 2.2 \times 10^{-16}$; (f): instrumental data for JAS mean temperature from Niğde and Konya 1951–2001, $r^2=0.428$, $p=1.919 \times 10^{-7}$ (based on Wainwright, Ayala 2018).*